Monitoring Transport Phenomena of Paramagnetic Metal-Ion Complexes Inside Catalyst Bodies with Magnetic Resonance Imaging

Jaap A. Bergwerff,[a] Anna A. Lysova,[b, c] Leticia Espinosa-Alonso,[a] Igor V. Koptyug,[b] and Bert M. Weckhuysen*[a]

Abstract: An indirect magnetic resonance imaging (MRI) method has been developed to determine in a noninvasive manner the distribution of paramagnetic Co^{2+} complexes inside Co/Al_2O_3 catalyst extrudates after impregnation with Co^{2+}/citrate solutions of different pH and citrate concentrations. UV/Vis/NIR microspectroscopic measurements were carried out simultaneously to obtain complementary information on the nature of the Co^{2+} complexes. In this way, it could be confirmed that the actual distribution of Co^{2+} inside the extrudates could be derived from the MRI images. By combining these space- and time-resolved techniques, information was obtained on both the strength and the mode of interaction between $[Co(H_2O)_6]^{2+}$ and different Co^{2+} citrate complexes with the Al_2O_3 support. Complexation of Co^{2+} by citrate was found to lead to a stronger interaction of Co with the support surface and formation of an egg-shell distribution of Co^{2+} complexes after impregnation. By addition of free citrate and by changing the pH of the impregnation solution, it was possible to obtain the rather uncommon egg-yolk and egg-white distributions of Co^{2+} inside the extrudates after impregnation. In other words, by carefully altering the chemical composition and pH of the impregnation solution, the macrodistribution of Co^{2+} complexes inside catalyst extrudates could be fine-tuned from eggshell over egg white and egg yolk to uniform.

Keywords: cobalt · magnetic resonance imaging · supported catalysts · UV/Vis spectroscopy

Introduction

The preparation of supported catalysts is an important industrial process, since these materials are used in crucial chemical processes such as hydrogenation reactions, Fischer–Tropsch synthesis, and hydrotreatment processes. The vast scale on which they are employed means that their preparation must be achieved by simple means.[1] In general, porous support bodies are impregnated with a solution containing metal-ion complexes, after which drying is carried out to deposit the precursor salts of the active phase on the support. Variations in the procedures used for impregnation and drying can have severe consequences for the activity of the final catalyst. The dispersion of the active phase and its macrodistribution inside the catalyst bodies are important parameters in this respect.[2–3] A number of studies in this field have led to a basic understanding of the physicochemical processes that take place during the preparation of supported catalyst bodies.[4–8] Models have even been derived that allow one to describe the effect of parameters such as the drying rate and the metal ion/support interaction on the macrodistribution of the metal-ion precursor in the dried catalyst bodies.[4, 6, 7]

Industrial impregnation solutions usually consist of a number of components, each with its own interaction with the support surface. Besides metal precursor salts, organic complexing agents such as citric acid and nitrilotriacetic acid are often added to impregnation solutions.[9–11] Different metal chelate complexes can thus be formed in the impregnation solution depending on pH and concentration. Moreover, it has been shown that pH gradients can occur inside catalyst bodies after impregnation, which can be expected to

[a] Dr. J. A. Bergwerff, L. Espinosa-Alonso, Prof. Dr. B. M. Weckhuysen
Inorganic Chemistry and Catalysis Group
Department of Chemistry, Faculty of Science, Utrecht University
Sorbonnelaan 16, 3584 CA Utrecht (The Netherlands)
Fax: (+31) 30-251-1027
E-mail: b.m.weckhuysen@uu.nl

[b] Dr. A. A. Lysova, Prof. Dr. I. V. Koptyug
International Tomography Center SB Ras
3A Institutskaya Street, Novosibirsk 630090 (Russia)

[c] Dr. A. A. Lysova
Boreskov Institute of Catalysis Sb RAS
5 Ak. Lavrent'eva Prospekt, Novosibirsk 630090 (Russia)

Supporting information for this article is available on the WWW under http://www.chemeurj.org/ or from the author.

influence the interaction between metal-ion complexes and the support surface.[12] Finally, the different structures of the individual support materials lead to different transport rate of compounds through the support bodies. With the aid of the existing models, it is therefore impossible to make reliable predictions of the macrodistribution of all different components inside industrial catalyst bodies. Methods that allow one to monitor the preparation process on-line can therefore be of great help for more controlled preparation of supported catalysts.

The analysis of bisected catalyst bodies with spatially resolved spectroscopic techniques makes it possible to determine the distribution of the different components of the impregnation solution inside these samples during the preparation process.[12–16] The possibility to monitor the transport of different components inside catalyst bodies in a noninvasive manner was previously illustrated in a study in which the distribution of phosphate and Pt complexes was determined in a direct manner with a multinuclear (e.g., ^{31}P and ^{195}Pt) MRI technique.[17] Recently, we briefly reported how the distribution of paramagnetic $[Co(H_2O)_6]^{2+}$ complexes after impregnation of support bodies can be monitored quantitatively in a noninvasive manner via their destructive effect on the ^1H NMR signal of the water solvent in MRI measurements.[18] Here we present a full account and show that this novel MRI method in the field of heterogeneous catalysis is generally applicable to monitoring the macrodistribution of different types of Co^{2+} complexes inside Co/Al_2O_3 catalyst bodies. By adding citric acid to the impregnation solution and varying its pH, the macrodistribution of the Co^{2+} complexes in the impregnated extrudates could be varied from eggshell, through egg white and egg yolk, to uniform.

Table 1. Composition and pH of Co/citrate impregnation solutions used in this study, as well as speciation of Co^{2+} complexes (as determined by UV/Vis/NIR spectroscopy) and concentration of free citrate in these solutions.

Solution	Composition			Speciation	
	$[Co^{2+}]$ [M]	[CA] [M]	pH	Co^{2+} complexes	$citrH_x^{(4-x)-}$
Co(0.2)CA(0.2)-pH1	0.20	0.20	1.5	0.20 M $[Co(H_2O)_6]^{2+}$	0.20 M $citrH_4$
Co(0.2)CA(0.4)-pH1	0.20	0.40	1.2	0.20 M $[Co(H_2O)_6]^{2+}$	0.40 M $citrH_4$
Co(0.2)CA(1.0)-pH1	0.20	1.00	1.0	0.20 M $[Co(H_2O)_6]^{2+}$	1.00 M $citrH_4$
Co(0.2)CA(0.2)-pH5	0.20	0.20	5.0	0.20 M $[Co(citrH)(H_2O)_3]^-$	–
Co(0.2)CA(0.4)-pH5	0.20	0.40	5.0	0.14 M $[Co(citrH)_2]^{4-}$	0.06 M $citrH^{3-}$
				0.06 M $[Co(citrH)(H_2O)_3]^-$	
Co(0.2)CA(1.0)-pH5	0.20	1.00	5.0	0.20 M $[Co(citrH)_2]^{4-}$	0.60 M $citrH^{3-}$
Co(0.2)CA(0.2)-pH9	0.20	0.20	10.0	0.20 M $[Co(citr)(H_2O)_3]^{2-}$	–
Co(0.2)CA(0.3)-pH9	0.20	0.30	9.5	0.20 M $[Co(citr)(H_2O)_3]^{2-}$	0.10 M $citrH^{3-}$
Co(0.2)CA(0.4)-pH9	0.20	0.40	9.0	0.20 M $[Co(citr)(H_2O)_3]^{2-}$	0.20 M $citrH^{3-}$

Experimental Section

Pore-volume impregnation of cylindrical γ-Al_2O_3 extrudates with 3.85 mm diameter was carried out with 0.20 M Co^{2+} solutions. The BET surface area of the support was 149 $m^2 g^{-1}$ and its pore volume was 0.39 $mL g^{-1}$. The mean pore diameter determined by N_2 physisorption was 8 nm, and no macropores were present in the extrudates. X-ray fluorescence (XRF) analysis showed that S (0.45 wt % SO_3), Si (0.23 wt % SiO_2), Ca (0.05 wt % CaO), and Fe (0.04 wt % Fe_2O_3) were present as the main impurities. The point of zero charge (PZC) of this material was 7.8, as determined by potentiometric mass titrations.[19] In the impregnation solutions, which were prepared from $Co(NO_3)_2·6H_2O$ (Acros, p.a.), citric acid (Acros, p.a.), and NaOH (Merck, p.a.), the citrate concentration and the pH were varied. The designations of the different solutions used in this study, as well as their pH and composition, are listed in Table 1.

Two-dimensional (2D) ^1H MRI images were recorded on the impregnated extrudates during the ageing process. Dehydration of the wet extrudates was prevented by inclusion of a wet tissue in the NMR tube. The MRI measurements were performed on a Bruker Avance DRX 300 wide-bore spectrometer with imaging accessories at 300.13 MHz (^1H). For detection of the signal, a two-pulse spin-echo sequence was used. Slice selection was used to record the signal from a 2 mm thick slice of the extrudates. Frequency encoding was applied in the x direction with a spatial resolution of 139 μm. The application of phase-encoding gradients in the y direction resulted in a spatial resolution of 231 μm in this direction. The time required for the acquisition of a single 2D image was 4–5 min.

For UV/Vis/NIR microspectroscopic measurements, different Al_2O_3 extrudates of the same batch were impregnated with the solutions listed in Table 1. The extrudates were bisected at different points in time after impregnation, and UV/Vis/NIR spectra were recorded on the bisected extrudates in the UV/Vis/NIR microspectroscopy setup described in previous work.[12] Pore-volume impregnation was also carried out on crushed Al_2O_3 extrudates with the same impregnation solutions. UV/Vis/NIR spectra were recorded on these samples in diffuse-reflectance mode on a Cary 500 spectrophotometer equipped with an integrating sphere and a white Halon standard as reference. The pH of the wet powders was determined with the aid of a spear-tip electrode.[19]

To help interpret the results, a simplified model was used to derive an estimation of the macrodistribution of different compounds inside the extrudates. In this model, the impregnation of a slab-shaped support body was mimicked by calculations. The distribution of components in the impregnation solution with different adsorption equilibrium constants K_{ads} and concentrations c_{imp} was estimated after impregnation for different positions inside the virtual support body. The slab was divided into different sections, each having the same (pore) volume and containing the same number of adsorption sites n_{ads}. The transport of different components through the support was simulated by assuming stepwise penetration of the impregnation solution into the slab. In the first step, the Al_2O_3 surface in the first section was contacted with the impregnation solution. The adsorption of the different components on the Al_2O_3 surface in this section was determined under the assumption of Langmuir adsorption and a constant concentration of components (equal to c_{imp}). Subsequently, the unadsorbed fraction of the different components was allowed to travel to the second section, while the first section was again exposed to the impregnation solution. The total concentration of a certain component in the first section was then equal to the amount adsorbed in the first step plus the concentration in the impregnation solution. The adsorption of the components in the different sections was again determined for the new situation in which the total concentration of the components has changed. Typically, the distribution of the components after seven adsorption and transport steps was determined. By varying the K_{ads} and c_{imp} values for the different components, the distribution of Co^{2+} complexes and citrate inside extrudates could be simulated to mimic the situation in the extrudates under study.

Results and Discussion

Speciation of Co²⁺ citrate complexes in aqueous solution: Since the interaction between the different components in the impregnation solution and the support surface is an important parameter, insight into the constitution of the impregnation solution is essential for controlled preparation of supported catalysts.[8] Up to now, the formation of Co²⁺ citrate complexes in aqueous solution has mainly been addressed from a biochemical point of view.[20,21] Formation constants for Co²⁺ citrate complexes were derived by potentiometric titrations for solutions with a low concentration of citrate (0.002–0.004 M).[20] Crystal structures of various Co²⁺ citrate complexes were deter-

Figure 1. Speciation of $[Co(H_2O)_6]^{2+}$ (○), $[Co(citrH_n)(H_2O)_3]^{(2-n)-}$ ($n=1, 2$) (▲), $[Co(citrH)_2]^{4-}$(×), and $[Co(citr)(H_2O)_3]^{2-}$ (□) complexes in 0.20 M Co solutions with different citrate concentrations (bottom) and the molecular structure of the Co²⁺ citrate complexes (top).

mined and used to propose structures of these complexes in solution. However, the use of formation constants derived from measurements on dilute solutions to predict the composition of more concentrated solutions is not without risk. Therefore, potentiometric titrations and UV/Vis/NIR spectroscopy were applied to validate the speciation of Co²⁺ citrate complexes in aqueous solution. Details of this study are given in the Supporting Information. The main results are summarized in Figure 1. Under the acidic conditions prevailing in solutions prepared from citric acid and Co(NO₃)₂ as the only ingredients, protonation of the citrate carboxylate groups is nearly complete, no complexation takes place between Co²⁺ and citrate, and $[Co(H_2O)_6]^{2+}$ complexes are mainly present. At a pH of approximately 5–6, the carboxylate groups of citrate are completely deprotonated and Co²⁺ citrate complexes can be formed with a Co:citrate ratio of 1:1 ($[Co(citrH)(H_2O)_3]^-$) and 1:2 ($[Co(citrH)_2]^{4-}$), depending on the amount of citrate available. Formation of these complexes from $[Co(H_2O)_6]^{2+}$ and citric acid is described by Equations (1) and (2). Coordination of Co²⁺ probably takes place through two carboxylate groups and the hydroxyl group, as shown in Figure 1. Formation of 1:1 Co²⁺ citrate complexes was observed in Co²⁺/citrate solutions of pH higher than 8, regardless of the amount of citrate available for complexation.
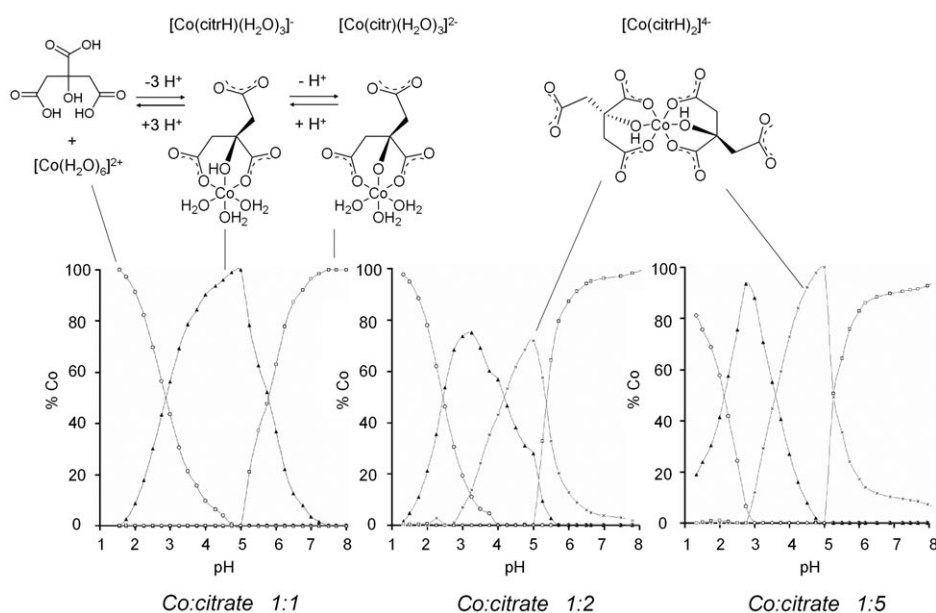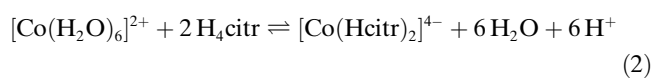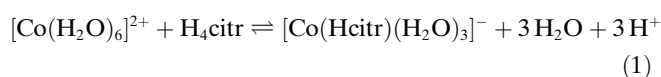
$$[Co(H_2O)_6]^{2+} + H_4citr \rightleftharpoons [Co(Hcitr)(H_2O)_3]^- + 3H_2O + 3H^+ \quad (1)$$

$$[Co(H_2O)_6]^{2+} + 2H_4citr \rightleftharpoons [Co(Hcitr)_2]^{4-} + 6H_2O + 6H^+ \quad (2)$$

Probably, $[Co(citr)(H_2O)_3]^{2-}$ complexes are formed in which coordination takes place through two carboxylate groups and a deprotonated hydroxyl group. The formation of this complex from $[Co(citrH)(H_2O)_3]^-$ is shown in Equation (3). For the different Co²⁺ complexes that can be present in aqueous solution, the positions of their characteristic UV/Vis/NIR bands are listed in Table 2.
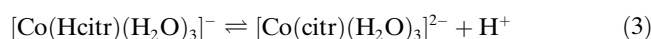
$$[Co(Hcitr)(H_2O)_3]^- \rightleftharpoons [Co(citr)(H_2O)_3]^{2-} + H^+ \quad (3)$$

Table 2. Positions and extinction coefficients of the most intense UV/Vis/NIR absorption bands for relevant Co²⁺ complexes in aqueous solution.

Complex	UV/Vis/NIR bands [nm]	Extinction coefficient [M⁻¹cm⁻¹]
$[Co(H_2O)_6]^{2+}$	511	4.4
$[Co(citrH_2)(H_2O)_3]$ $[Co(citrH)(H_2O)_3]^-$	513	9.2
$[Co(citrH)_2]^{4-}$	509	13.4
$[Co(citr)(H_2O)_3]^{2-}$	534	14.1
	727	2.2

Reference spectra of the different Co²⁺ complexes were used to fit the UV/Vis/NIR spectra recorded on 0.20 M Co solutions of different pH and citrate concentration. In this way, the speciation of these complexes in 1:1, 1:2, and 1:5 Co²⁺:citrate solutions was determined as a function of pH. The resulting speciation plots are shown in Figure 1. From these plots, the nature and concentration of the different components in the impregnation solutions used in this study could be derived. Cobalt:citrate solutions at pH 1 (CoCA-pH1) were found to contain $[Co(H_2O)_6]^{2+}$ and a varying

amount of citrH$_4$. It proved to be impossible to distinguish between [Co(citrH$_2$)(H$_2$O)$_3$] and [Co(citrH)(H$_2$O)$_3$]$^-$ complexes by UV/Vis/NIR spectroscopy, since the only difference between these complexes is the protonation state of the free carboxylate group. Since deprotonation of the carboxylate groups is complete at this pH, the Co(0.2)CA(0.2)-pH5 solution almost exclusively contained [Co(citrH)-(H$_2$O)$_3$]$^-$. Approximately 70% of all Co in the Co(0.2)CA-(0.4)-pH5 solution is present as [Co(citrH)$_2$]$^{4-}$, while it was assumed that the Co(0.2)CA(1.0)-pH5 solution merely contained this complex and free citrate. In the CoCA-pH9 solutions, [Co(citr)(H$_2$O)$_3$]$^{2-}$ was exclusively present. Besides this complex, the Co(0.2)CA(0.3)-pH9 and Co(0.2)CA(0.4)-pH9 solutions contained varying amounts of free citrate. The estimated concentrations of free citrate and Co^{2+} complexes in the impregnation solutions are included in Table 1.

Impregnation with CoCA-pH1 solutions: When a support material is exposed to an aqueous solution, protonation and deprotonation of the surface hydroxyl groups can lead to a shift in the pH of this solution. Especially when impregnation is carried out without excess solution, this buffering effect can be substantial. To determine the effect of the support on the pH of the solution inside the Al$_2$O$_3$ pores, pH measurements were carried out on crushed Al$_2$O$_3$ extrudates after impregnation with different solutions. The thus-obtained pH values are listed in Table 3. When impregnation

Table 3. pH of the impregnation solution before and after impregnation of crushed Al$_2$O$_3$ extrudates.

Solution	pH before	pH after
Co(0.2)CA(0.2)-pH1	1.5	3.3
Co(0.2)CA(0.4)-pH1	1.2	2.5
Co(0.2)CA(0.2)-pH5	5.0	7.1
Co(0.2)CA(0.4)-pH5	5.0	7.0
Co(0.2)CA(0.2)-pH9	10.0	8.0
Co(0.2)CA(0.4)-pH9	9.5	8.8

was carried out with CoCA-pH1 solutions, protonation of the Al$_2$O$_3$ surface led to an increase in pH to a value of 2.5–3.3. Due to this buffering effect of the support, the pH increases to a value at which Al$_2$O$_3$ is stable against dissolution. The UV/Vis/NIR spectra recorded on crushed extrudates after impregnation with Co(0.2)CA(0.4) solutions of different pH are shown in Figure 2. In this figure, the spectrum of Al$_2$O$_3$ powder impregnated with a 0.2 M Co(NO$_3$)$_2$ solution is included for comparison. In this spectrum, the maximum of the Co^{2+} d–d band is located at 525 nm. The observed red shift compared to the spectrum of [Co-(H$_2$O)$_6$]$^{2+}$ in solution (maximum at 511 nm) can be explained by the exchange of water ligands for support hydroxyl groups and the formation of inner-sphere complexes between [Co(H$_2$O)$_6$]$^{2+}$ and the Al$_2$O$_3$ surface.[22–25] The spectrum recorded on Al$_2$O$_3$ impregnated with the Co(0.2)CA-(0.4)-pH1 solution shows a d–d band with lower intensity and a maximum at 515 nm. This spectrum resembles that of [Co(H$_2$O)$_6$]$^{2+}$ in solution, which points to limited chemical
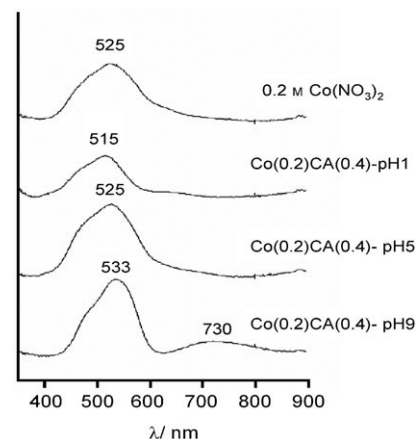

Figure 2. UV/Vis/NIR spectra of crushed Al$_2$O$_3$ extrudates after impregnation with (from top to bottom) 0.2 M Co(NO$_3$)$_2$, Co(0.2)CA(0.4)-pH1, Co(0.2)CA(0.4)-pH5, and Co(0.2)CA(0.4)-pH9 solutions.

interaction between these complexes and the support after impregnation. In aqueous solutions, an increase in pH to a value of 2.5–3.3 was found to lead to deprotonation of citric acid and formation of Co^{2+} citrate complexes (Figure 1). Complexation by citrate leads to an increase in the extinction coefficient of the Co^{2+} d–d transition band (Table 2). Judging from the low intensity of the absorption band in the spectrum recorded on Al$_2$O$_3$ impregnated with the Co-(0.2)CA(0.4)-pH1 solution, it seems that, despite the increase in pH, hardly any Co^{2+} citrate complexes were formed inside the Al$_2$O$_3$ matrix.

An indirect MRI method was used to determine the distribution of paramagnetic complexes in catalyst bodies. It was shown before that after impregnation the extrudates are instantaneously filled with the impregnation solution, and a homogeneous distribution of water, and therefore protons, is present throughout the support bodies.[17] At the same time, transport of components in the impregnation solution that can be adsorbed on the support surface is hampered, and these compounds remain near the outer surface of the support bodies. The presence of paramagnetic complexes leads to a decrease in the relaxation times of water protons. Since signal detection is achieved with a spin-echo pulse sequence, a short relaxation time results in a decrease in the ^{1}H NMR signal. The accumulation of paramagnetic components in certain areas of the extrudates can therefore be inferred from a low local ^{1}H NMR signal.

Two-dimensional ^{1}H MRI images recorded on extrudates at several points in time after impregnation with CoCA-pH1 solutions of different citrate concentrations are presented in Figure 3a. In these images, the ^{1}H NMR signal intensity is indicated by different colors, where red indicates low signal intensity and blue high signal intensity. Hence, in general, areas in the catalyst bodies with a high concentration of Co^{2+} complexes are shown in red. One-dimensional profiles of the ^{1}H NMR signal intensity as a function of the position inside the extrudates after impregnation with 0.20 M Co-(NO$_3$)$_2$ and Co(0.2)CA(0.4)-pH1 solutions are depicted in
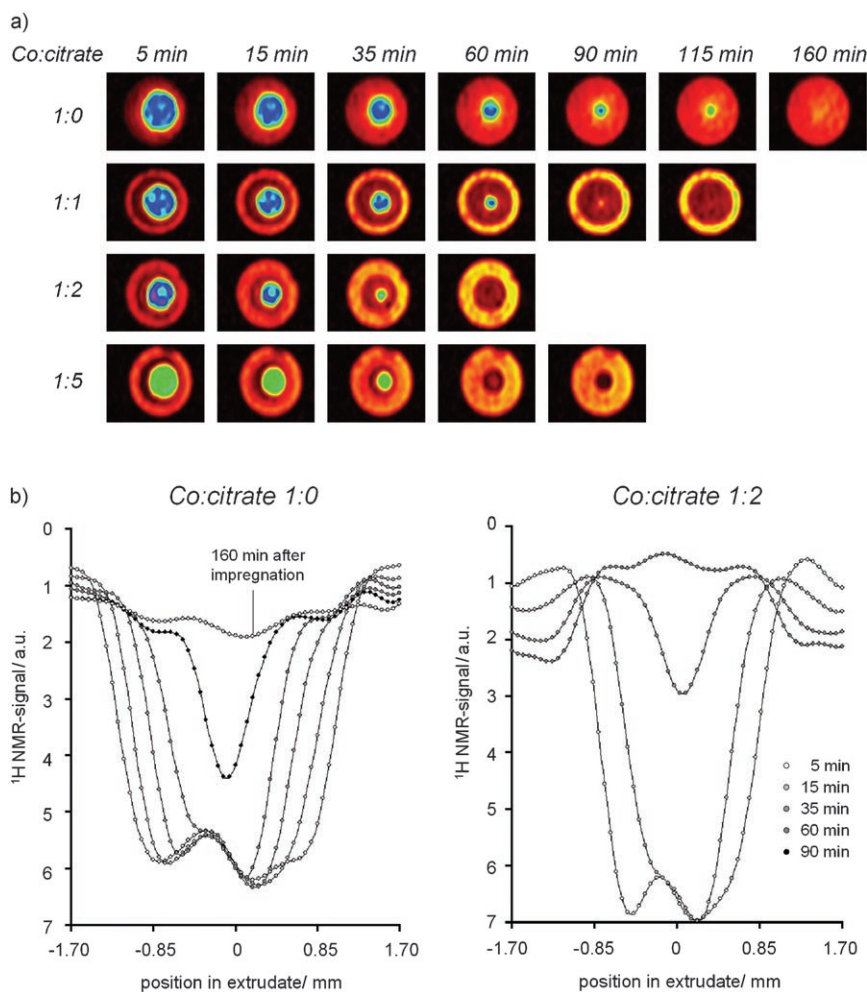
Figure 3. a) 2D ^{1}H MRI images recorded on Al_2O_3 extrudates after impregnation with (from top to bottom) 0.2 M $Co(NO_3)_2$, Co(0.2)CA(0.2)-pH1, Co(0.2)CA(0.4)-pH1, and Co(0.2)CA(1.0)-pH1 solutions. b) 1D profiles of the ^{1}H NMR signal intensity as a function of position inside Al_2O_3 extrudates after impregnation with 0.2 M $Co(NO_3)_2$ and Co(0.2)CA(0.4)-pH1 solutions.

Figure 3b. In these profiles, the *y* axis shows the ^{1}H NMR signal intensity in reversed order, to mimic the distribution of Co^{2+} complexes. In this figure, images and profiles of an Al_2O_3 extrudate after impregnation with a $Co(NO_3)_2$ solution are included for comparison. Transport of Co^{2+} complexes from the edge towards the center of the extrudates was clearly observed as a shrinking core of high ^{1}H NMR signal intensity. The addition of citric acid had two effects. First, as compared to the $Co(NO_3)_2$ solution, the presence of $[Co(H_2O)_6]^{2+}$ at the center of the extrudate was observed at a shorter time after impregnation. Apparently, addition of citric acid led to an increase in the transport rate of Co^{2+} complexes inside the Al_2O_3 extrudates. Second, the formation of a ring with higher NMR signal intensity was observed near the protruding Co front. This is most clearly observed in the 1D profiles obtained from the extrudate impregnated with the Co(0.2)CA(0.4)-pH1 solution. Ninety minutes after impregnation with all CoCA-pH1 solutions, images were obtained in which the ^{1}H NMR signal intensity is higher near the external surface of the extrudates, which

would imply an egg-yolk distribution of Co^{2+} complexes inside the extrudates. This implies that Co^{2+} interacts in the same way at the edges and the center.

To verify that this type of distribution was actually established, extrudates were bisected 2 h after impregnation with the different CoCA-pH1 solutions for visual inspection. In all cases, Co^{2+} complexes were present throughout the extrudates, since the entire cross section had a pink color. Besides, an outer ring of a lighter color was indeed observed. The inner diameter of this ring decreased with increasing citrate concentration in the impregnation solution, in line with the ^{1}H MRI measurements. For a photograph of a bisected extrudate 2 h after impregnation with the Co-(0.2)CA(1.0)-pH 1 solution, see Figure S8 in the Supporting Information.

To explain the faster transport of $[Co(H_2O)_6]^{2+}$ and the formation of an egg-yolk distribution of Co^{2+} complexes, the interaction of citrate and $[Co(H_2O)_6]^{2+}$, the two components in the impregnation solutions, with the protonated Al_2O_3 surface must be evaluated. At low pH, citrate is known to react strongly with Al_2O_3 surfaces.[26] Adsorption of citrate probably takes place on Al^{3+} surface sites after release of the hydroxyl group from the Al_2O_3 surface. Since H_2O is a better leaving group than OH^-, adsorption predominantly takes place on protonated hydroxyl groups. The reaction of citrate with Al_2O_3 surface hydroxyl groups is described in Equation (4). Exchange of one or more water ligands of the $[Co(H_2O)_6]^{2+}$ complex for support oxygen atoms can lead to chemical adsorption of $[Co(H_2O)_6]^{2+}$ onto the Al_2O_3 surface [Eq. (5)].[22]

$$citrH^{3-} + Al_SOH_2{}^+ \xrightarrow{K_{ads}(citrH^{3-})} Al_S-Hcitr^{2-} + H_2O \qquad (4)$$

$$[Co(H_2O)_6]^{2+} + x\,Al_SOH \underset{}{\overset{K_{ads}([Co(H_2O)_6]^{2+})}{\rightleftharpoons}}$$
$$[(Al_SO)_xCo(H_2O)_{(6-x)}]^{(2-x)+} + x\,H^+ \qquad (5)$$
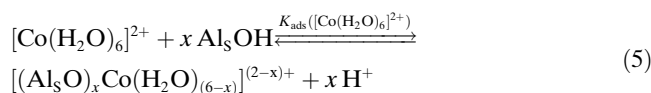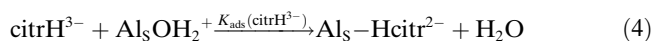
The observed faster transport of Co^{2+} complexes on addition of citric acid may partially result from weaker interac-

tion between $[Co(H_2O)_6]^{2+}$ and the Al_2O_3 surface. The low pH of the impregnation solution means that the equilibrium in Equation (5) is shifted to the left and formation of inner-sphere Co surface complexes is suppressed. This is in line with the UV/Vis/NIR measurements, which also pointed to limited interaction between $[Co(H_2O)_6]^{2+}$ complexes and the Al_2O_3 surface after impregnation with the Co(0.2)CA(0.4)-pH1 solution (Figure 2). The formation of a ring of high Co concentration and the establishment of an egg-yolk distribution can be explained by assuming that the adsorption of $[Co(H_2O)_6]^{2+}$ complexes is hampered by the presence of adsorbed citrate on the Al_2O_3 surface. Adsorption of both citrate and $[Co(H_2O)_6]^{2+}$ takes place on surface hydroxyl groups as described in Equations (4) and (5). However, the surface of γ-Al_2O_3 is known to contain a number of different hydroxyl groups. Their acid/base properties are determined by the coordination of the surface oxygen atoms. From Equations (4) and (5), it is obvious that basic hydroxyl groups are more reactive towards the adsorption of citrate, while acidic hydroxyl groups are most likely involved in the formation of inner-sphere Co^{2+} surface complexes. Nevertheless, adsorption of citrate apparently hinders adsorption of $[Co(H_2O)_6]^{2+}$ on neighboring adsorption sites. Since at low pH $K_{ads}(citrH^{3-})$ is larger than $K_{ads}([Co(H_2O)_6]^{2+})$, adsorbed citrate is probably located in a ring near the external surface of the extrudate just after impregnation. Towards the center of the extrudate, the citrate concentration decreases, more surface sites are available for the adsorption of $[Co(H_2O)_6]^{2+}$, and the surface density of Co surface complexes can be higher. A similar mechanism was previously proposed to explain egg-yolk Pt distributions in the preparation of Pt/Al_2O_3 pellets.[27] The processes taking place inside an Al_2O_3 extrudate after impregnation with CoCA-pH1 solutions are schematically depicted in Figure 4a. A simplified model, explained in the Experimental Section, was used to estimate the distribution of citrate and $[Co(H_2O)_6]^{2+}$ inside Al_2O_3 extrudates after impregnation. In this model, adsorption of both citrate and Co^{2+} complexes is assumed to take place on a single type of surface site, which is a gross simplification, as discussed above. Nevertheless, the competitive adsorption model allows one to describe the distribution of citrate and Co complexes inside impregnated extrudates in a qualitative manner. The situation approximately 35 min after impregna-
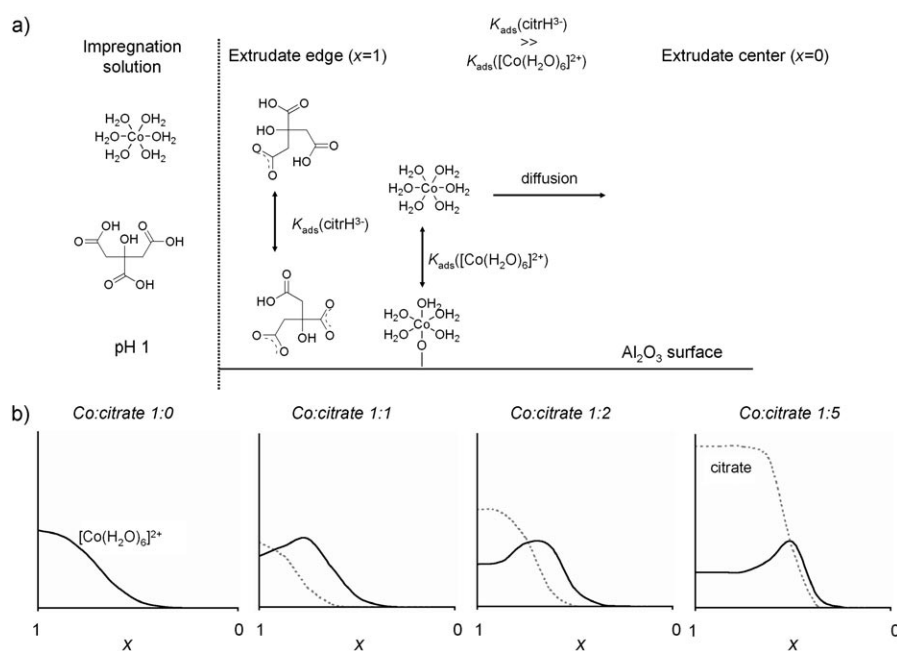

Figure 4. Schematic representation of the processes taking place inside an Al_2O_3 extrudate after impregnation with CoCA-pH1 solutions (a) and estimated distribution of $[Co(H_2O)_6]^{2+}$ (solid lines) and citrate (dotted lines) inside Al_2O_3 extrudates 35 min after impregnation (b).

tion with the different CoCA-pH1 solutions is depicted in Figure 4b.

Impregnation with CoCA-pH5 solutions: Impregnation of crushed extrudates with CoCA-pH5 solutions led to an increase in pH of the impregnation solution inside the pores to 7.0. The UV/Vis/NIR spectrum recorded on Al_2O_3 powder impregnated with a Co(0.2)CA(0.4)-pH5 solution shows a d–d band with a maximum at 525 nm (Figure 2). Despite the pH increase, formation of $[Co(citr)(H_2O)_3]^{2-}$, the stable complex in aqueous solution at pH 7.0, was not observed inside the Al_2O_3 pores, since no absorption band was observed at 730 nm in the UV/Vis/NIR spectrum.

Figure 5a shows 2D ^{1}H MRI images obtained from extrudates after impregnation with the CoCA-pH5 solutions of different Co:citrate ratios. The 1D ^{1}H NMR signal-intensity profiles obtained from extrudates after impregnation with Co(0.2)CA(0.2)-pH5 and Co(0.2)CA(1.0)-pH5 solutions are presented in Figure 5b. Since the Co(0.2)CA(0.2)-pH5 solution merely contains $[Co(citrH)(H_2O)_3]^-$ (Figure 1), the measurements on extrudates impregnated with this solution can be used to determine the interaction between this complex and the Al_2O_3 surface. Impregnation with a Co(0.2)CA-(0.2)-pH5 solution resulted in formation of a sharp ring of low ^{1}H NMR signal intensity near the external surface of the extrudates immediately after impregnation. Only slight broadening of this ring was observed after ageing for 15 h. A photograph of an extrudate that was bisected at this time after impregnation (Figure 6) shows that the observed ^{1}H NMR signal intensity profile indeed corresponds to a
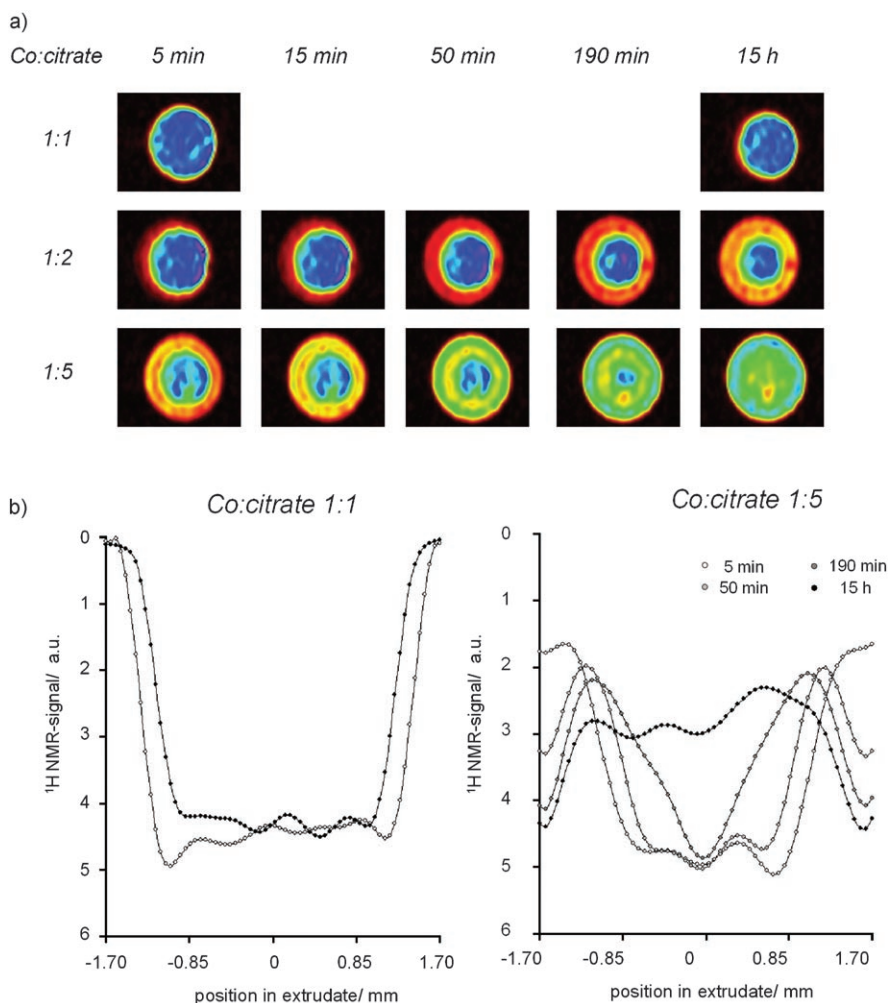
Figure 5. a) 2D ^{1}H MRI images recorded on Al_2O_3 extrudates after impregnation with (from top to bottom) Co(0.2)CA(0.2)-pH5, Co(0.2)CA(0.4)-pH5, and Co(0.2)CA(1.0)-pH5 solutions. b) 1D profiles of the ^{1}H NMR signal intensity as a function of position inside Al_2O_3 extrudates after impregnation with Co(0.2)CA(0.2)-pH5 and Co(0.2)CA(1.0)-pH5 solutions.
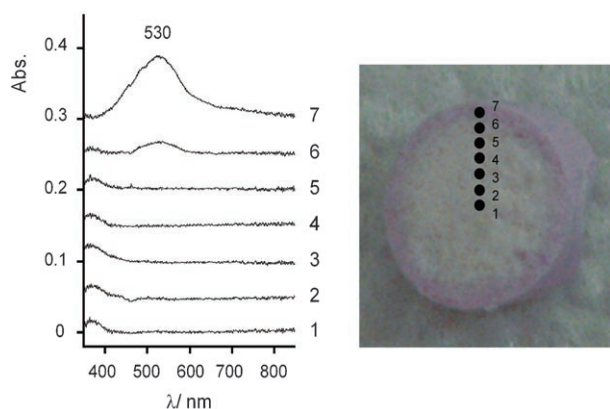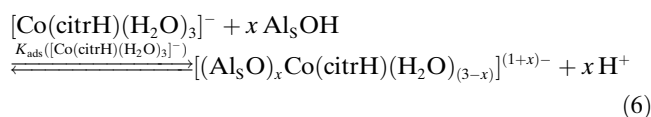

Figure 6. UV/Vis/NIR spectra recorded on an Al_2O_3 extrudate bisected 15 h after impregnation with a Co(0.2)CA(0.2)-pH5 solution. The locations of the measurement spots are indicated in the photograph.

sharp eggshell distribution of Co^{2+} complexes. UV/Vis/NIR spectra recorded on this bisected extrudate are also included

in Figure 6. An absorption band due to Co^{2+} d–d transitions is only observed in the spectrum recorded near the external surface of the extrudate. Even at 48 h after impregnation, the 2D MRI image reveals an eggshell distribution of Co^{2+} complexes inside the extrudate (not shown).

From the slow transport of $[Co(citrH)(H_2O)_3]^-$, it can be seen that a strong interaction exists between this complex and the support surface. Adsorption of $[Co(citrH)(H_2O)_3]^-$ complexes onto the Al_2O_3 surface may take place in different ways. First, impregnation with the slightly acidic solution may lead to protonation of the hydroxyl groups and creation of a positively charged surface. The increase in pH that was observed upon impregnation of the Al_2O_3 powder is probably a result of this surface protonation. An electrostatic interaction could exist between the surface and negatively charged $[Co(citrH)(H_2O)_3]^-$, as was evidenced previously for $[H_xPtCl_6]^{(2-x)-}$ and a protonated Al_2O_3 surface.[28–29] However, considering its low negative charge, the observed interaction between $[Co(citrH)(H_2O)_3]^-$ and the support seems too strong to be explained by purely electrostatic interactions. Exchange of water ligands for support hydroxyl groups can lead to formation of inner-sphere surface complexes, as expressed in Equation (6). From this equation, it is clear that adsorption of $[Co(citrH)(H_2O)_3]^-$ on the Al_2O_3 surface leads to liberation of protons. Nevertheless, a net pH increase is observed after impregnation with the Co-(0.2)CA(0.2)-pH5 solution. Apparently, protonation of basic Al_2O_3 hydroxyl groups has a dominant effect on the pH of the solution inside the Al_2O_3 pores. The UV/Vis/NIR spectrum recorded near the external surface of the extrudate impregnated with the Co(0.2)CA(0.2)-pH5 solution (Figure 6) shows an absorption band with maximum at 530 nm. The spectrum of $[Co(citrH)(H_2O)_3]^-$ in aqueous solution shows a band at 513 nm. This shift is a further argument for chemical interaction between $[Co(citrH)(H_2O)_3]^-$ and the support. Apparently, the coordination of Co^{2+} by citrate makes the remaining water ligands more easily exchangeable for hydroxyl groups.

$$[\text{Co(citrH)(H}_2\text{O)}_3]^- + x\,\text{Al}_S\text{OH}$$

$$\underset{K_{ads}([\text{Co(citrH)(H}_2\text{O)}_3]^-)}{\rightleftharpoons}[(\text{Al}_S\text{O})_x\text{Co(citrH)(H}_2\text{O)}_{(3-x)}]^{(1+x)-} + x\,\text{H}^+$$

$$(6)$$

When the citrate concentration in the impregnation solution is increased, the transport of Co^{2+} complexes proceeds at a higher rate. Furthermore, the formation of a ring of higher ^{1}H NMR signal intensity near the external surface of the extrudate is observed. This phenomenon is most pronounced in the 1D ^{1}H NMR signal-intensity profile obtained 50 min after impregnation with the Co(0.2)CA(1.0)-pH5 solution (Figure 5b). When the Co^{2+} complexes have reached the center of the extrudates, an egg-yolk distribution is again obtained, judging form the higher ^{1}H NMR signal intensity observed for positions at the periphery of the extrudate 15 h after impregnation with the Co(0.2)CA(1.0)-pH5 solution.

In the Co(0.2)CA(0.4)-pH5 and Co(0.2)CA(1.0)-pH5 solutions, most of the Co^{2+} is contained in $[\text{Co(citrH)}_2]^{4-}$ (Figure 1). The UV/Vis/NIR spectrum of this complex in aqueous solution shows a band with a maximum at 509 nm (Table 2). The absorption band in the UV/Vis/NIR spectrum of the crushed extrudates impregnated with Co(0.2)CA(0.4)-pH5 (Figure 2) is located at 525 nm. Apparently, after impregnation, disintegration of the $[\text{Co(citrH)}_2]^{4-}$ complex takes place inside the Al_2O_3 pores. The adsorption of citrate on the Al_2O_3 surface [Eq. (4)] probably leads to a lower citrate concentration inside the Al_2O_3 pores and formation of $[\text{Co(citrH)(H}_2\text{O)}_3]^-$ complexes adsorbed on alumina at the expense of $[\text{Co(citrH)}_2]^{4-}$, which has an absorption band at 525 nm (Figure 6). In the following discussion, it is assumed that $[\text{Co(citrH)(H}_2\text{O)}_3]^-$ and free citrate are the only components inside the Al_2O_3 pores after impregnation with the Co(0.2)CA(0.4)-pH5 and Co-(0.2)CA(1.0)-pH5 solutions, despite the presence of $[\text{Co-}(\text{citrH})_2]^{4-}$ in the impregnation solution.

A strong interaction between citrate and an Al_2O_3 surface was reported when impregnation was carried out with a citrate solution of pH 5. At this pH, ample protonated hydroxyl groups are available for reaction with citrate. Furthermore, the citrate carboxylate groups are deprotonated, and this allows for strong coordination of the Al^{3+} sites. As was discussed for the CoCA-pH1 solutions, the presence of adsorbed citrate may hinder adsorption of Co complexes onto the Al_2O_3 surface for steric reasons. The differences in adsorption strength between citrate (strong) and $[\text{Co(citrH)-}(\text{H}_2\text{O)}_3]^-$ (slightly weaker) may explain the faster transport of the Co^{2+} complexes when impregnation was carried out with Co(0.2)CA(0.4)-pH5 and Co(0.2)CA(1.0)-pH5 solutions. However, as compared to the $[\text{Co(H}_2\text{O)}_6]^{2+}$ in the CoCA-pH1 solutions, in this case, a stronger interaction exists between $[\text{Co(citrH)(H}_2\text{O)}_3]^-$ and the Al_2O_3 surface. During the diffusion of $[\text{Co(citrH)(H}_2\text{O)}_3]^-$ towards the center of the extrudate, adsorption of this complex takes place as soon as adsorption sites are available. As a result, during the ageing process, the formation of a sharp ring of low ^{1}H NMR signal intensity is observed at the position of the advancing Co front. When this extrudate was allowed to age for 15 h, an egg-yolk distribution of $[\text{Co(citrH)(H}_2\text{O)}_3]^-$ resulted. At this point in time, an eggshell distribution of Hcitrate^{3-} is still present, but $[\text{Co(citrH)(H}_2\text{O)}_3]^-$ complexes have distributed themselves evenly over the remaining adsorption sites. The processes described above are summarized in Figure 7a. The estimated distributions of $[\text{Co(citrH)-}(\text{H}_2\text{O)}_3]^-$ and citrate inside Al_2O_3 extrudates 190 min after impregnation with different CoCA-pH5 solutions are shown in Figure 7b.

Impregnation with CoCA-pH9 solutions: A slight decrease in pH to a value of 8.0–8.8 was observed after impregnation with the CoCA-pH9 solutions. Since the pH of these solutions is close to the PZC of the support, impregnation has little effect on the pH of the solution inside the pores. The UV/Vis/NIR spectrum of $[\text{Co(citr)(H}_2\text{O)}_3]^{2-}$, present in all CoCA-pH9 solutions, shows two distinct bands at 534 and 727 nm (Table 2). These bands are also observed in the spec-
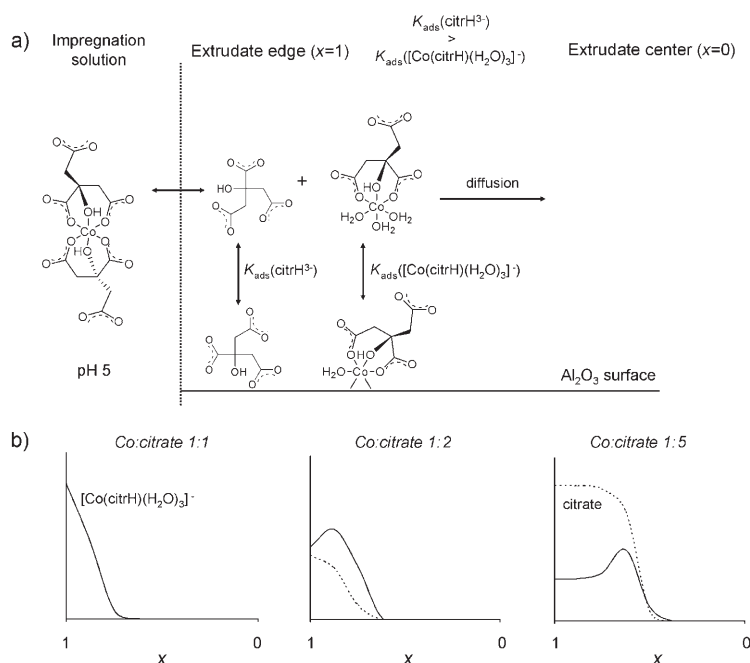

Figure 7. Schematic representation of the processes taking place inside an Al_2O_3 extrudate after impregnation with a Co(0.2)CA(0.4)-pH5 solution (a) and estimated distribution of $[\text{Co(citrH)(H}_2\text{O)}_3]^-$ (solid lines) and citrate (dotted lines) inside Al_2O_3 extrudates 190 min after impregnation with different CoCA-pH5 solutions (b).

trum recorded on the Al_2O_3 powder impregnated with the Co(0.2)CA(0.4)-pH9 solution, as shown in Figure 2. Apparently, the structure of the Co^{2+} citrate complex remained largely intact after impregnation. The 2D ^1H MRI images and the corresponding 1D profiles of the ^1H NMR signal intensity as a function of position inside the extrudates, recorded at different times after impregnation with Co-(0.2)CA(0.2)-pH9, Co(0.2)CA(0.3)-pH9, and Co(0.2)CA-(0.4)-pH9 solutions, are presented in Figure 8 a and b, respectively.

The distribution of Co^{2+} complexes after impregnation with the Co(0.2)CA(0.2)-pH9 solution provides information on the interaction of $[Co(citr)(H_2O)_3]^{2-}$ with the Al_2O_3 surface. Slow transport of Co^{2+} complexes was observed in this case. Even 48 h after impregnation, no constant ^1H NMR signal was observed for all positions inside the extrudate, and from the intensity of the signal near the core of the extrudate it is clear that no paramagnetic complexes are present at this position. The presence of an eggshell distribution of Co^{2+} complexes is confirmed by the photograph of a bi-

sected extrudate, taken 120 min after impregnation with a Co(0.2)CA(0.2)-pH9 solution (Figure 9, top left). UV/Vis/NIR microspectroscopy measurements (not shown) indicated that only $[Co(citr)(H_2O)_3]^{2-}$ complexes were present near the external surface of this extrudate. Since the pH of the impregnation solutions was close to the PZC of the support, the Al_2O_3 surface was probably neutrally charged after impregnation with the CoCA-pH9 solutions. Hence, the observed strong interaction between $[Co(citr)(H_2O)_3]^{2-}$ and the Al_2O_3 surface can only be explained by a ligand-exchange mechanism, as expressed in Equation (7). This complex appears to be less strongly adsorbed than $[Co(Hcitr)-(H_2O)_3]^-$ after impregnation with the Co(0.2)CA(0.2)-pH5 solution. In comparison to the impregnation of Al_2O_3 extrudates with the Co(0.2)CA(0.2)-pH5 solution, transport of Co^{2+} complexes proceeded at a higher rate at pH 9.

$$[Co(citr)(H_2O)_3]^{2-} + x\,Al_SOH$$
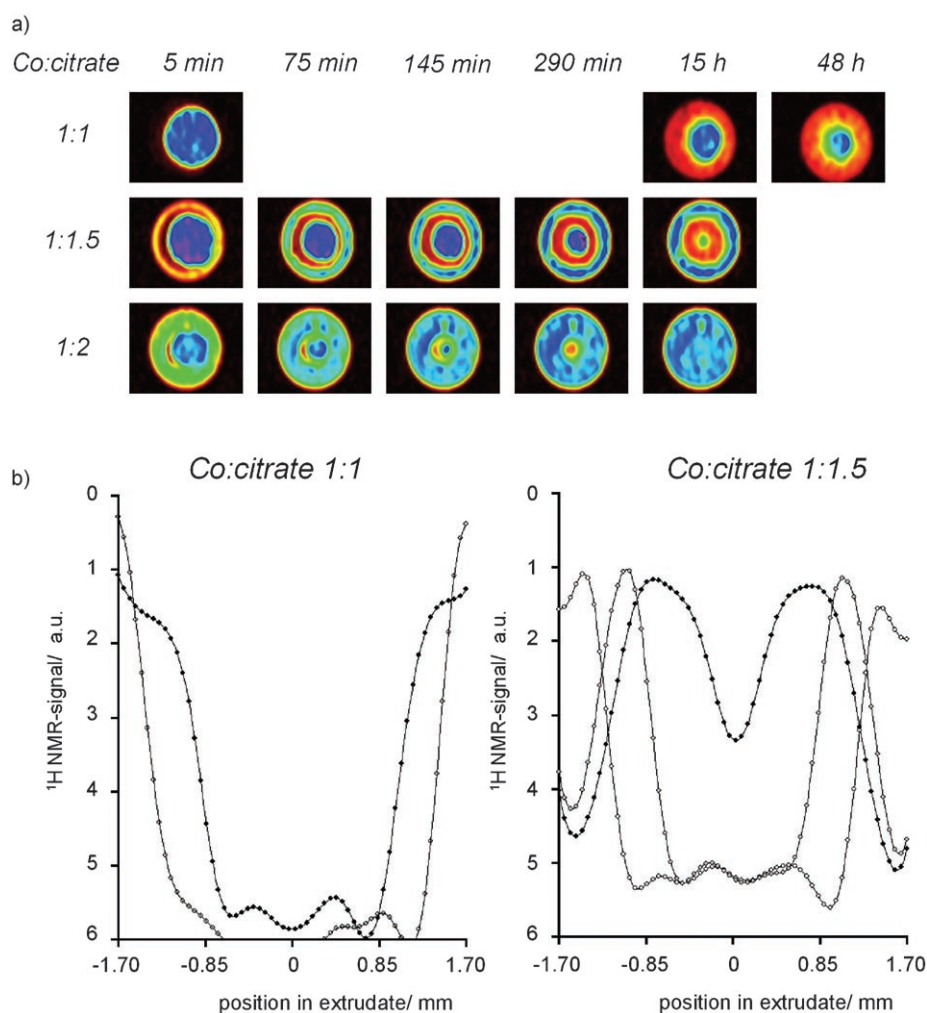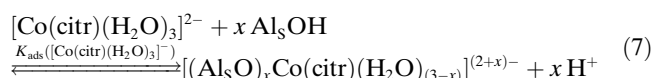$$\xrightleftharpoons[K_{ads}([Co(citr)(H_2O)_3]^-)]{}[(Al_SO)_x Co(citr)(H_2O)_{(3-x)}]^{(2+x)-} + x\,H^+ \quad (7)$$

Figure 8. a) 2D ^1H MRI images recorded on Al_2O_3 extrudates after impregnation with (from top to bottom) Co(0.2)CA(0.2)-pH9, Co(0.2)CA(0.3)-pH9 and Co(0.2)CA(0.4)-pH9 solutions. b) 1D profiles of the ^1H NMR signal intensity as a function of position inside Al_2O_3 extrudates after impregnation with Co(0.2)CA(0.2)-pH9 and Co(0.2)CA(0.3)-pH9 solutions.

Again, an increase in the citrate concentration of the impregnation solution leads to faster transport of Co^{2+} complexes. The size of the area with a high ^1H NMR signal intensity near the core of the extrudates (where no Co^{2+} complexes are present) decreases at a faster rate when impregnation is carried out with Co-(0.2)CA(0.3)-pH9 and Co-(0.2)CA(0.4)-pH9 solutions. This trend is also illustrated in Figure 9, where photographs recorded on bisected extrudates 120 min after impregnation are shown, together with the corresponding 2D ^1H MRI images. The domains where no Co^{2+} complexes were present are labeled "a" in these images. A ring with low ^1H NMR intensity is observed at the edges of the extrudate impregnated with the Co-(0.2)CA(0.2)-pH9 solution and at positions near the advancing Co front when impregnation is carried out with the Co-(0.2)CA(0.3)-pH9 and Co-(0.2)CA(0.4)-pH9 solutions. These areas are indicated by "b". In the corresponding photographs, a ring with a darker color is indeed observed at
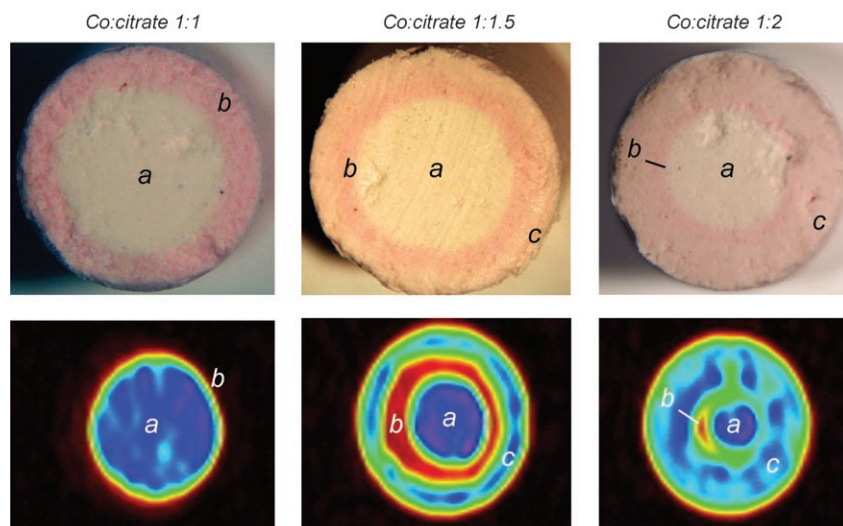
Figure 9. Photographs (top) and 2D ^{1}H MRI images (bottom) recorded on Al$_2$O$_3$ extrudates 120 min after impregnation with (from left to right) Co(0.2)CA(0.2)-pH9, Co(0.2)CA(0.3)-pH9 and Co(0.2)CA(0.4)-pH9 solutions.

tions where Co^{2+} complexes are present (positions 5–7). Only [Co(citr)(H$_2$O)$_3$]$^{2-}$-type complexes seem to be present inside the wet extrudates. The higher intensity of the d–d bands in spectra at positions 5 and 6 shows that a slightly higher concentration of these complexes is present near the Co front. At the same time, the ^{1}H NMR signal at these positions is drastically decreased. Apparently, the destructive effect of [Co(citr)-(H$_2$O)$_3$]$^{2-}$ on the ^{1}H NMR signal is strongly enhanced above a certain concentration. Possibly, [Co(citr)(H$_2$O)$_3$]$^{2-}$ in solution has a much larger effect on the ^{1}H NMR signal than adsorbed [Co(citr)-(H$_2$O)$_3$]$^{2-}$, since their paramagnetic Co^{2+} cations are more exposed to the water molecules. The presence of a high concentration of unadsorbed complexes near the Co front could explain the low ^{1}H NMR signal intensity observed at these positions.

these positions. Towards the edges of the extrudates, a ring with a lighter color is seen, which is labeled "c". In the corresponding 2D MRI images a stronger signal is found for these positions. Fifteen hours after impregnation with a Co-(0.2)CA(0.4)-pH9 solution, a constant signal is found throughout the extrudate. The intensity of the ^{1}H NMR signal is only slightly lower than what was observed for an extrudate filled with water. Apparently, the Co^{2+} cations present in areas labeled "c" are effectively shielded from the water protons, and their destructive effect on the ^{1}H NMR signal is minimized.

To determine the nature of the Co^{2+} complexes present in regions a–c inside the extrudates, UV/Vis/NIR spectra were recorded on an extrudate bisected 120 min after impregnation with a Co(0.2)CA(0.3)-pH9 solution. The thus-obtained spectra are presented in Figure 10. The positions of the measurement spots are indicated in the photograph. Bands are observed at 537 and 720 nm in all spectra recorded at posi-
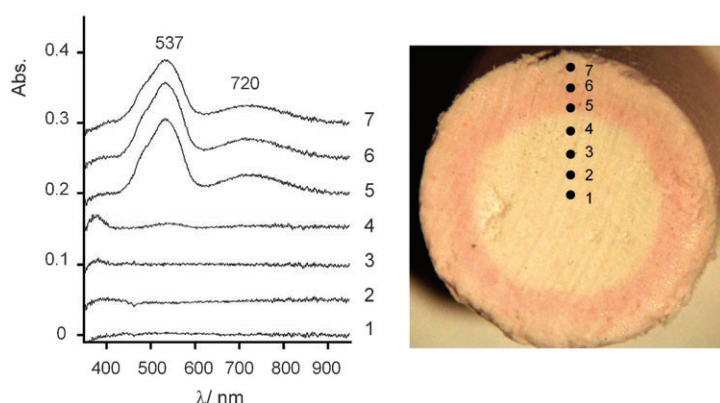
The presence of additional citrate in the Co(0.2)CA(0.3)-pH9 and Co(0.2)CA(0.4)-pH9 solutions leads to faster transport of Co^{2+} complexes and formation of a ring with higher Co concentration near the protruding Co front. When impregnation was carried out with CoCA solutions of pH 1 and 5, the manifestation of these phenomena could be explained by assuming a mechanism in which adsorption of citrate onto the Al$_2$O$_3$ surface decreases the number of adsorption sites for Co^{2+} complexes. After adsorption of citrate, neighboring surface sites are blocked through steric hindrance. For this explanation to be valid, an eggshell distribution of citrate must be present, and K_{ads}(citrH^{3-}) needs to be larger than the adsorption equilibrium constants of the Co^{2+} complexes, a reasonable assumption at low pH. However, at high pH, weak interaction between citrate and the Al$_2$O$_3$ surface is reported in the literature. In a separate set of MRI experiments on ^{13}C-labeled citrate impregnation chemistry (not shown for brevity), a homogeneous distribution of citrate was observed almost immediately after impregnation of Al$_2$O$_3$ extrudates with a 0.40 M trisodium citrate solution of pH 9. This fast transport can be the result of a decrease in the number of adsorption sites available for adsorption of citrate, rather than a decrease in K_{ads}(citrH^{3-}). In comparison, the Co(0.2)CA(0.3)-pH9 (0.1 M citrH^{3-}) and Co(0.2)CA(0.4)-pH9 (0.2 M citrH^{3-}) solutions contain a lower concentration of free citrate (Table 1). Hence, an inhomogeneous distribution of citrate may still be present in the first hours after impregnation with these solutions. Nevertheless, occupation by citrate of a small percentage of the hydroxyl groups in the external area of the extrudates still

Figure 10. UV/Vis/NIR spectra recorded on an Al$_2$O$_3$ extrudate bisected 120 min after impregnation with a Co(0.2)CA(0.3)-pH9 solution. The locations of the measurement spots are indicated in the photograph.

renders a large fraction of the hydroxyl groups available for adsorption of [Co(citr)-(H$_2$O)$_3$]$^{2-}$ and is unlikely to affect the adsorption of these complexes to any great extent. The situation changes when it is assumed that adsorption of citrate hinders adsorption of [Co(citr)(H$_2$O)$_3$]$^{2-}$ through electrostatic repulsion between adsorbed citrate and negatively charged [Co(citr)(H$_2$O)$_3$]$^{2-}$. The extended effect of electrostatic interactions could imply that the adsorption of citrate hinders the adsorption of Co^{2+} complexes on a large number of surface sites.

The relevant processes that occur inside an Al$_2$O$_3$ extrudate after impregnation with a Co(0.2)CA(0.4)-pH9 solution are illustrated schematically in Figure 11a. When blocking of [Co(citr)(H$_2$O)$_3$]$^{2-}$ adsorption sites by citrate was assumed, the distribution of citrate and [Co(citr)(H$_2$O)$_3$]$^{2-}$ complexes inside extrudates after impregnation with the different CoCA-pH9 solutions could be derived by using the simple model to describe impregnation. The resulting concentration profiles 120 min after impregnation are presented in Figure 11b.

Figure 11. Schematic representation of the processes taking place inside an Al$_2$O$_3$ extrudate after impregnation with a Co(0.2)CA(0.4)-pH9 solution (a) and the estimated distribution of [Co(citr)(H$_2$O)$_3$]$^{2-}$ (solid lines) and citrate (dotted lines) inside Al$_2$O$_3$ extrudates 120 min after impregnation with different CoCA-pH9 solutions (b).

Conclusion

The combined application of magnetic resonance imaging and UV/Vis/NIR microspectroscopy provided unique complementary information on the chemical nature and space- and time-resolved distribution of Co^{2+} complexes inside Al$_2$O$_3$ extrudates. In all cases, the obtained Co^{2+} distribution inside Al$_2$O$_3$ extrudates could be derived from the ^{1}H MRI images, which further illustrates the potential of the MRI technique in catalyst preparation studies. In this way, the formation of eggshell, eggyolk, egg-white, and uniform distributions of the Co^{2+} precursor complexes could be elegantly observed. While UV/Vis/NIR microspectroscopy provides molecular information on the Co^{2+} complexes
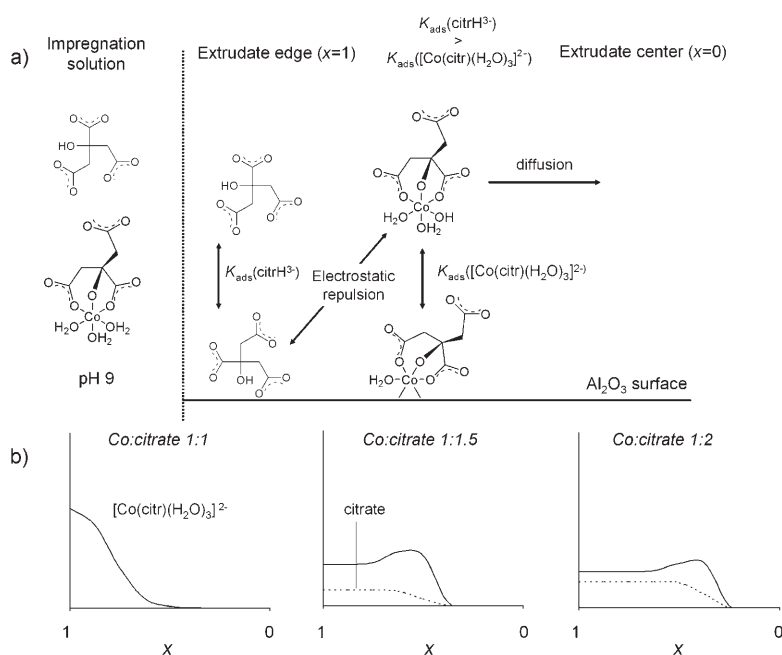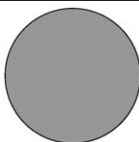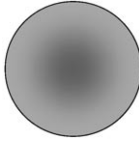
inside the Al$_2$O$_3$ matrix obtained after bisecting extrudates at specific times during impregnation or drying, the macrodistribution of Co^{2+} complexes inside the extrudates and the dynamics of the impregnation process could be determined by the MRI technique in a noninvasive manner.

In general, it was found that the addition of citrate to the impregnation solutions had two effects. First, complexation of citrate with Co^{2+} resulted in a considerable increase in the interaction between the Co precursor and the support. As a result, (sharp) eggshell Co distributions were established after impregnation with solutions that merely contained Co^{2+} citrate complexes. This is illustrated in the top part of Table 4, which schematically shows the macrodistri-

Table 4. Effect of the strength of the metal ion/support interaction and the presence of a competitive adsorbent on the macrodistribution of the metal-ion precursor in impregnated extrudates.

		Adsorption strength of metal-ion precursor		
		strong	medium	weak
Competitive adsorption of citrate	absent	extreme eggshell	eggshell	uniform
	present		egg white	egg yolk

bution of metal-ion complexes as a function of their adsorption strength. Second, competitive adsorption between Co^{2+} complexes and free citrate resulted in faster transport of metal-ion complexes towards the center of the extrudates. The stronger interaction between free citrate and the Al_2O_3 surface led to establishment of an eggshell distribution of this component after impregnation. Near the exterior surface of the extrudates, fewer sites were now available for adsorption of Co^{2+} complexes, and the Co^{2+} complexes were found to diffuse faster to the center of the extrudates. Eggwhite and egg-yolk distributions of Co were formed during ageing. The effect of adding to the impregnation solution a component that is adsorbed strongly on the Al_2O_3 surface on the macrodistribution of metal-ion complexes inside extrudates is schematically depicted in the bottom part of Table 4. By varying pH and citrate concentration in the impregnation solutions, the macrodistribution of Co^{2+} complexes inside Al_2O_3 extrudates could be controlled.

Acknowledgements

[1] a) *Preparation of Solid Catalysts* (Eds.: G. Ertl, H. Knozinger, J. Weitkamp), Wiley-VCH, Weinheim, **1999**; b) J. Hagen, *Industrial Catalysis, A Practical Approach*, Wiley-VCH, Weinheim, **1999**; c) *Catalyst Preparation: Science and Engineering* (Ed.: J. Regalbuto), CRC Press, Boca Raton, **2007**.

[2] A. T. Bell, *Science* **2003**, *299*, 1688.

[3] R. Schlögl, S. B. Abd Hamid, *Angew. Chem.* **2004**, *116*, 1656; *Angew. Chem. Int. Ed.* **2004**, *43*, 1628.

[4] S. Y. Lee, R. Aris, *Catal. Rev. Sci. Eng.* **1985**, 27, 207.

[5] A. V. Neimark, L. I. Kheifez, V. B. Fenelonov, *Ind. Eng. Chem. Prod. Res. Dev.* **1981**, 20, 439.

[6] A. Lekhal, B. J. Glasser, J. G. Khinast, *Chem. Eng. Sci.* **2001**, *56*, 4473.

[7] A. Lekhal, B. J. Glasser, J. G. Khinast, *Chem. Eng. Sci.* **2004**, *59*, 1063.

[8] K. Bourikas, C. Kordulis, A. Lycourghiotis, *Catal. Rev. Sci. Eng.* **2006**, 48, 363.

[9] A. J. van Dillen, R. Terorde, D. J. Lensveld, J. W. Geus, K. P. de Jong, *J. Catal.* **2003**, *216*, 257.

[10] F. Negrier, E. Marceau, M. Che, *Chem. Commun.* **2002**, 1194.

[11] J. Y. Carriat, M. Che, M. Kermarec, M. Verdaguer, A. Michalowicz, *J. Am. Chem. Soc.* **1998**, *120*, 2059.

[12] L. G. A. van de Water, J. A. Bergwerff, T. A. Nijhuis, K. P. de Jong, B. M. Weckhuysen, *J. Am. Chem. Soc.* **2005**, *127*, 5024.

[13] J. A. Bergwerff, T. Visser, B. R. G. Leliveld, B. D. Rossenaar, K. P. de Jong, B. M. Weckhuysen, *J. Am. Chem. Soc.* **2004**, *126*, 14548.

[14] J. A. Bergwerff, M. Jansen, B. R. G. Leliveld, T. Visser, K. P. de Jong, B. M. Weckhuysen, *J. Catal.* **2006**, *243*, 292.

[15] J. A. Bergwerff, L. G. A. van de Water, T. Visser, P. de Peinder, B. R. G. Leliveld, K. P. de Jong, B. M. Weckhuysen, *Chem. Eur. J.* **2005**, *11*, 4591.

[16] L. G. A. van de Water, G. L. Bezemer, J. A. Bergwerff, M. Versluijs-Helder, B. M. Weckhuysen, K. P. de Jong, *J. Catal.* **2006**, *242*, 287.

[17] A. A. Lysova, I. V. Koptyug, R. Z. Sagdeev, V. N. Parmon, J. A. Bergwerff, B. M. Weckhuysen, *J. Am. Chem. Soc.* **2005**, *127*, 11916.

[18] J. A. Bergwerff, A. A. Lysova, L. Espinosa Alonso, I. V. Koptyug, B. M. Weckhuysen, *Angew. Chem.* **2007**, *119*, 7362; *Angew. Chem. Int. Ed.* **2007**, *46*, 7224.

[19] J. Park, J. R. Regalbuto, *J. Colloid Interface Sci.* **1995**, *175*, 239.

[20] N. Kotsakis, C. P. Raptopoulou, V. Tangoulis, A. Terzis, J. Giapintzakis, T. Jakusch, T. Kiss, A. Salifoglou, *Inorg. Chem.* **2003**, *42*, 22.

[21] M. Matzapetakis, M. Dakanali, C. P. Raptopoulou, V. Tangoulis, A. Terzis, N. Moon, J. Giapintzakis, A. Salifoglou, *J. Biol. Inorg. Chem.* **2000**, *5*, 469.

[22] J. Vakros, K. Bourikas, S. Perlepes, C. Kordulis, A. Lycourghiotis, *Langmuir* **2004**, *20*, 10542.

[23] T. Ataloglou, C. Fountzoula, K. Bourikas, J. Vakros, A. Lycourghiotis, C. Kordulis, *Appl. Catal. A* **2005**, 288, 1.

[24] T. Ataloglou, J. Vakros, K. Bourikas, C. Fountzoula, C. Kordulis, A. Lycourghiotis, *Appl. Catal. B* **2005**, 57, 299.

[25] T. Ataloglou, K. Bourikas, J. Vakros, C. Kordulis, A. Lycourghiotis, *J. Phys. Chem. B* **2005**, *109*, 4599.

[26] P. C. Hidber, T. J. Graule, L. J. Gauckler, *J. Am. Ceram. Soc.* **1996**, *79*, 1857.

[27] P. Papageorgiou, D. M. Price, A. Gavriilidis, A. Varma, *J. Catal.* **1996**, *158*, 439.

[28] W. A. Spieker, J. Liu, X. Hao, J. T. Miller, A. J. Kropf, J. R. Regalbuto, *Appl. Catal. A* **2003**, 243, 53.

[29] W. A. Spieker, J. R. Regalbuto, *Chem. Eng. Sci.* **2001**, *56*, 3491.